INSTITUTE OF PHYSICS PUBLISHING JOURNAL OF OPTICS A: PURE AND APPLIED OPTICS

J. Opt. A: Pure Appl. Opt. **3** (2001) 255–261 www.iop.org/Journals/oa PII: S1464-4258(01)17016-9

Circulating loop simulations for transmission performance comparison of various node architectures

Edward Mutafungwa

Communications Laboratory, Otakaari 8, PL 2300, Helsinki University of Technology, FIN-02015 HUT, Finland

E-mail: edward.mutafungwa@hut.fi

Received 11 September 2000, in final form 8 March 2001

Abstract

Optical cross-connect system comparisons are carried out in this paper with an emphasis on the transmission performance of different node architectures. We employ a photonic simulator to bypass the considerable cost and time constraints that would arise if a similar task was carried out in a laboratory. The computation times are minimized by using an optical circulating loop to create a simplified simulation configuration of an optical network. Based on the simulation results, the estimated upper limit on the number of cascadable 2×2 nodes is obtained for different node architectures and performance targets. Almost twice as many nodes can be traversed by a signal in systems with nodes that employ novel switching technologies characterized by high crosstalk isolation (higher than 55 dB) and/or low insertion losses compared to earlier proposed monolithically integrated node designs.

Keywords: Cross-connect nodes, optical switching, WDM systems, simulation crosstalk, fibre nonlinearities

(Some figures in this article are in colour only in the electronic version; see `www.iop.org`)

1. Introduction

Future communication transport networks are likely to consist of an edge network made up of various client signal networks such as ATM networks, SDH (or SONET) rings, etc. The various signal formats, (e.g., ATM cells, IP datagrams, GbE frames etc), emanating from these client networks are aggregated, routed and managed in an underlying wavelength-division multiplexing (WDM) based protocol-independent core network shown in figure 1. This enables the clients to take advantage of the abundant transmission capacity and flexibility, provided courtesy of the optical networking employed within the core network [1].

One of the most essential enabling technologies for optical networking is the optical cross-connect node (OXN) [2, 3], whose primary function is the cross-connection of the constituents of a WDM aggregate signal arriving via a set of input fibre links to their corresponding outgoing fibre links (figure 2). Moreover, the wavelength reconfiguration capability offered by OXNs enables the network operator to adjust to any traffic fluctuations, ease network congestion, accommodate physical growth of the network and rapidly restore services in the event of a failure(s) occurring within the network.

In a practical physical network topology, a transmitted optical signal is likely to traverse several nodes along a designated optical path between any non-adjacent source–destination node pair. This is accompanied by the signal impairment attributed to factors such as fibre nonlinearities, dispersion, accumulated amplifier noise and saturation [2]. Additionally, noise and crosstalk induced or leaked by the node subsystems (e.g., switches, amplifiers, multiplexers), may lead to further degradation of the signal quality if they happen to lie within the signal's carrier bandwidth [4] or even interact with fibre nonlinearities [5]. The node induced impairments place an upper limit on the number of traversable nodes before electrical regeneration becomes necessary, hence, restricting a full implementation of transparent optical networking. For instance, a request to re-route a signal along an alternative path, so as to avoid congestion, may be denied if the number of OXNs lying on the back-up path exceeds a certain limit.

A variety of OXNs have been reported by various research and development groups (see [3, 6] and references quoted therein). The cascadability limit of each node type differs

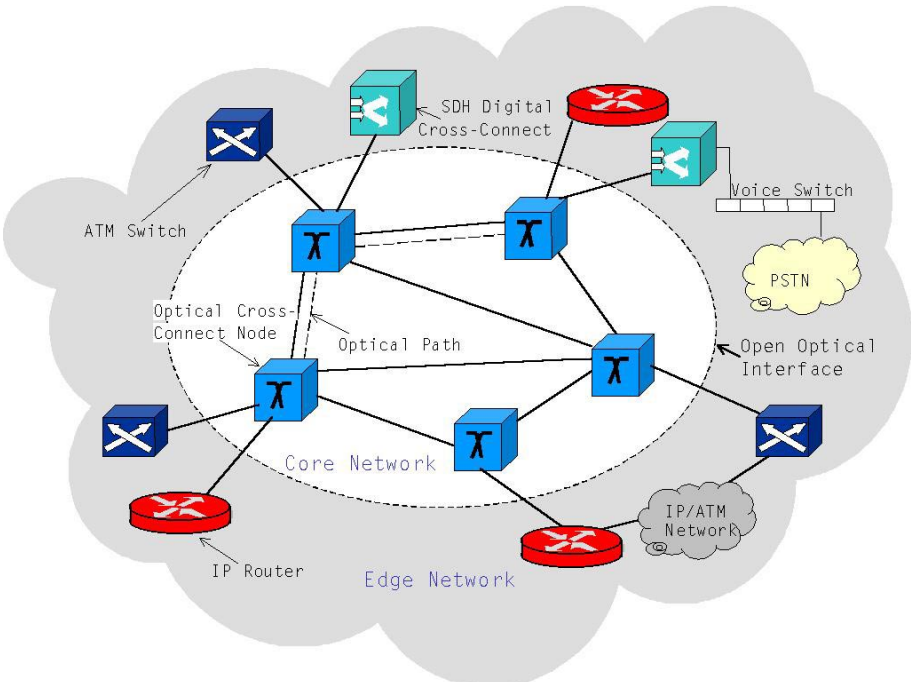

Figure 1. Conceptual architecture of future communication transport networks.

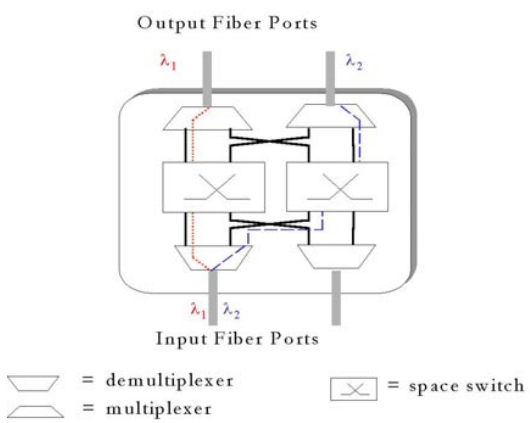

Figure 2. The basic 2 × 2 OXN configuration for a two channel system (λ_1 is passed through while λ_2 is cross-connected).

according to the extent of the performance imperfections of their subsystems, node dimensions or size. Among the major issues tackled in a network's preliminary design stage is included the selection of a node-type capable of handling all optical path requests whilst meeting a certain performance criterion. Furthermore, any unforeseen post-deployment node reconfigurations due to increase in capacity demand, path re-routing requests and alterations to the physical topology should be carried without significant performance deterioration. Therefore, the network designer's decision on the OXN architecture to be deployed is based on a number of operational characteristics that include blocking characteristics, scalability/modularity, latency and transmission performance. Investigation of some of those characteristics is usually aided by results obtained from experimental testbeds or field trials that involve the OXN.

This particular task of comparing the transmission performance of various OXNs would prove costly, time consuming and requires sizeable manpower, if it were to be performed in a hardware laboratory environment. By sidestepping these time and cost constraints, computer-aided modelling tools ease the analysis of diverse or complex systems. However, a majority of commercially available optical simulators require long computation times, thus limiting their practicality to system-level (point-to-point link) simulations [7]. In this paper, we devise a computational efficient system-level simulation routine that could be used for larger optical networks and use it to estimate the number of 2 × 2 (2 input/output fibre ports) OXNs that can be cascaded for a given performance threshold.

2. Proposed OXN nodes

The various OXN architectures can be classified according to their blocking characteristics (strictly non-blocking, rearrangably non-blocking or blocking), routing strategy adapted (wavelength or virtual wavelength path routing), inherent modularity (link or wavelength modularity), device technology or architectural configuration [6]. A majority of the proposed nodes have the configuration of the OXN shown in figure 2 which offers inherent wavelength modularity and has been successfully implemented in digital cross-connect systems [3].

For this study, we select seven OXN architectures that are fairly representative of the numerous proposals that have been made. Since the main emphasis is on analysing transmission performance, an OXN classification according to performance-influencing devices or components is adopted. These nodes (and their respective codenames adopted for the remainder of this paper) are:

(a) OXN1: using switches based on bubbles generated in fluid-filled trenches on silica waveguides (also known as champagne switches [8]). A 2×2 switch has an insertion loss of 2.74 dB and a 70 dB isolation (crosstalk attenuation).
(b) OXN2: using 2×2 titanium-diffused lithium niobate ($Ti:LiNbO_3$) electro-optic switches, each switching element having a 3 dB loss (including fibre coupling losses) and an isolation of 30 dB [6, 9].
(c) OXN3: based on bulk optics and movable switchplates that create frustrated total internal reflection used for switching purposes [10]. Early tests on a 1×2 switch of this type indicated an isolation of less than 55 dB and insertion of under 1 dB [10].
(d) OXN4: utilizing compact micro-electro mechanical systems (MEMS) that switch signals by deflecting them using 2-D arrays of movable mirrors erected on a silicon substrate [11]. A 2×2 implemented using a single mirror has a loss of 0.6 dB and isolation of above 50 dB [12].
(e) OXN5: having an alternative configuration to the OXN of figure 2 and switches signal using strain tunable fibre Bragg gratings (FBGs) as well as dual (de)multiplexing array waveguide gratings (AWGs) [13]. The FBGs have a loss, 3 dB bandwidth and reflectivity of 0.1 dB, 0.4 nm and 99% respectively. Polarization dependent AWGs are assumed, with a centre channel insertion loss of 2.5 dB and isolation of 40 dB for a 100 GHz channel spacing [15].
(f) OXN6: using delivery and coupling switches that constitute gated 1×2 Mach–Zehnder interferometric (MZI) electro-optic switches and thermo-optic phase-shifters on a silicon substrate [6, 14]. The MZI switch isolation is 30 dB and the on-chip loss is <1 dB.
(g) OXN7: consisting of phased array waveguide gratings monolithically integrated with 2×2 MZI switches on an InP substrate [16]. The MZI switches in this OXN have an isolation of 20 dB and the AWGs have specifications similar to those described in (e).

3. System modelling

In this section, the simulator's architecture and in-built device models are briefly outlined. The simulation set-up for OXN cascadability testing is illustrated and the crucial modelling parameters are also stated.

3.1. The PTDS tool overview

Simulations are carried out using the photonic transmission design suite (PTDS version 1.3 by Virtual Photonics Inc.) running on a Windows™ NT platform [17]. Within PTDS, the components that make up the OXN subsystems are imitated by custom or user-defined modules based on their individual numerical models. Optical and electrical signals are represented as computer data that are exchanged between interconnected modules via a simulation environment adaptation layer. The response of a module to input signals is obtained by evaluating their numerical models (written as basic C++ code) in the optical network simulation layer. Furthermore, an additional extensive mathematical module library enables further processing, visualization and analysis of the data obtained from a particular simulation run. As a prelude to the description of the OXN simulation task, a brief description of the primary modules and their underlying mathematical models in the simulation routines is outlined below.

3.1.1. Transmitter arrays The individual optical transmitter modules represent an externally modulated fixed-laser diode. The data source is provided by a PRBS generator, a non-return-to zero (NRZ) pulse coder, and a rise-time specification module. The laser diode produces a continuous wave light signal with an optical field represented by [19]

$$E(t) = \sqrt{P} \begin{pmatrix} \sqrt{1-k} \\ \sqrt{k}\exp(j\phi) \end{pmatrix} \cdot \exp\left(\mathrm{j}\int \omega(\tau)\,\mathrm{d}\tau\right), \quad (1)$$

where P is the signal power, k (lying in the interval [0, 1]) is the power splitting parameter between the polarization states, $\omega(\cdot)$ is a Gaussian white noise function, and ϕ is an additional phase related to azimuth angle $\wp$ of the output polarization by

$$\tan(2\wp) = 2\frac{\sqrt{k(1-k)}\cdot\cos\phi}{1-2k}. \quad (2)$$

A Mach–Zehnder modulator (MZM) is the default external modulator in the transmitter module. It includes adjustable parameters that allow the user to take into account the frequency chirp that occurs as a result of modulator asymmetry.

3.1.2. Optical amplifiers The erbium-doped fibre amplifiers were simulated using an amplification module with a wavelength independent gain (G) and noise figure (NF). This module may operate in a gain-controlled mode by using an internal control-loop to lock the gain to a user specified target and neglect the amplifier self-saturation due to amplified spontaneous emission (ASE) noise. Alternative modes are the power-controlled mode whereby the pump power is varied to maintain a constant output power and the saturation mode in which the amplifier is uncontrolled because all the parameters are kept constant for all conditions. Other adjustable amplifier parameters include the noise figure, saturation power and noise bandwidth. Solving the propagation equation that governs the amplification process over the amplifier length yields [2]

$$\ln G = \ln\left(\frac{P_{out}}{P_{in}}\right) = \ln G_0 - \frac{P_{in}(G-1)}{P_{sat}} \cdot \frac{G_0 \cdot \ln 2}{(G_0-2)}, \quad (3)$$

where P_{in} and P_{out} are the input and output power levels respectively, G_0 is the unsaturated gain and P_{sat} is the user defined saturation power. Similarly, given an ASE factor n_{sp} the amplifier noise figure (NF) modelled as

$$NF = 10\log\left(2n_{sp}\cdot\frac{G-1}{G} + \frac{1}{G}\right). \quad (4)$$

A forward pump configuration is assumed, alternative pump configurations are available with other amplifier modules.

3.1.3. Fibre waveguides The standard single-mode fibre (SMF) waveguide is simulated by a nonlinear dispersive fibre module. This models the signal propagation in the fibre by solving the nonlinear Schrödinger equation (NLSE) using the split-step Fourier method [20]. It takes into account Kerr nonlinearities, first and second order group-velocity dispersion and evaluates the frequency dependent fibre attenuation. Ignoring higher-order nonlinear effects, for pulses of a duration > 10 ps with a normalized amplitude of U at normalized space and time coordinates Z and T respectively, the NLSE can be expressed as [20]

$$\mathrm{j}\frac{\partial U}{\partial Z} - \frac{\operatorname{sgn}(\beta_2)}{2}\frac{\partial^2 U}{\partial T^2} + \mathrm{j}\frac{\beta_3}{6\,|\beta_2|\,T_0}\frac{\partial^3 U}{\partial T^3} + \gamma P_0 L_D\,|U|^2\,U = -\mathrm{j}\alpha L_D U \tag{5}$$

where α is the fibre attenuation coefficient, γ is the nonlinearity coefficient, P_0 and T_0 are the peak power and pulse width respectively, L_D is the dispersion length while $\beta_{2,3}$ denote the nonlinear propagation constants.

Adjustable numerical parameters offer an option for controlling the accuracy of the solution and evaluation speed. A dispersion compensation is implemented by redefining the attenuation, dispersion and effective core area parameters of the SMF module.

3.1.4. Wavelength multiplexers and demultiplexers The general $N \times 1$ wavelength multiplexer module is implemented using a total of N Bessel bandpass filters with distinct centre frequencies and an variable attenuator modelling the multiplexer insertion loss. A demultiplexer module consists of a similar number of filters preceded by a $1 \times N$ splitter and an attenuator. An exception is made for multiplexing and demultiplexing modules employing arrayed waveguide gratings (AWG) since they are modelled by the Gaussian approximation of the modal field within the waveguide [19].

3.1.5. Receiver and BER evaluation To model a PIN photodetector, a module is used to convert the optical field into an electrical signal using a user defined responsivity. The statistically independent noise currents (shot and thermal noise currents) are modelled as additive noise with the aid of Gaussian white noise generators. The receiver noise filtering is provided by a lowpass filter with a Gaussian transfer function, whereby the cutoff frequency and order of the filter are adjustable.

After a particular simulation run the system performance is established by numerically evaluating the Q factor (electrical signal-to-noise ratio) and/or bit error rate (BER) using a BER simulation module implementing a Gaussian approximation method with an optimum threshold setting and a module for ideal clock recovery. Assuming that I_i, σ_i represent the photocurrent and noise variance respectively for a received 'i' bit, the Q factor can be typically expressed as [2]

$$Q = \frac{|I_1 - I_0|}{\sigma_1 + \sigma_0}, \tag{6}$$

and considering an optimum threshold setting, it is related to the BER by [2]

$$\mathrm{BER} = \frac{\exp\left(-Q^2/2\right)}{Q\sqrt{2\pi}}. \tag{7}$$

3.2. Simulation configuration and parameters

Modelling of the OXNs is carried out on a 4-channel WDM system spanning λ_1–λ_4 and using the intensity modulated–direct detection (IM/DD) scheme. The bit rate per channel is set at 2.5 Gbit s^{-1} (OC-48) using a $2^{15} - 1$ PSRB word pattern. A channel spacing of 100 GHz is selected and the emission frequencies (in THz) of the transmitters are set at the assigned channels [192.95, 193.05, 193.15, 193.25]. The externally modulated transmitters have an extinction ratio of 30 dB and the maximum power per channel is 1 mW.

The simulation configuration comprises an optical circulating loop with the 2×2 OXN under test, as illustrated in figure 3. Circulating loops are used in hardware experimental set-ups to reduce cost by minimizing the amount of equipment required for an experiment. In system-level simulators, such as PTDS, the reduction in module number by the circulating loop minimizes the required computation time. For instance, in figure 3, simulating an N cascade of OXNs is similar to simulating $N - 1$ point-to-point fibre links that are an excerpt from the network. An equivalent full network-level simulation would involve up to $N(N-1)/2$ fibre links, and is likely to increase the computer time by factor of $N/2$. This is made even worse if dynamic traffic conditions are considered, where the simulations have to be re-run for each network state. Wavelength-domain simulators are better suited to network-level simulation, but their improved computation time is a result of reducing the details (less accuracy) embedded in the signals [7].

The loop consists of a SMF (ITU Recommendation G.652) fibre link and spool DCF (ITU Recommendation G.653) fibre links with an aggregate length of 35 km and simulation parameters indicated in table 1. A preamplifier (POA) precedes the OXN and operates in the gain controlled mode with a small signal gain of 9.2 dB and saturation output power set at 10 dBm. The boost amplifier (BOA) operates using the power controlled mode with an output power of 0 dBm. The receiver includes a PIN photodetector with a responsivity of 1 A W^{-1}, thermal noise of $10^{-12} A\,H_z^{-1/2}$ and a receiver filter bandwidth of 1.75 GHz.

In the above set-up (figure 3), the OXN under test is configured to cross-connect the paths of λ_1 and λ_3 from an incoming fibre port to diagonally located output fibre whilst channels λ_2 and λ_4 are passed through to their corresponding output fibre ports. By using this configuration, signals at channels λ_2 and λ_4 from the source node traverse all of the intermediate nodes (equivalent to the number of re-circulation loop cycles). This facilitates the assessment of node cascadability by carrying out the performance analysis of either one of these two channels at the destination node.

4. Simulation results and performance assessment

Received eye diagrams (normalized electrical signal) provide a comparison of the quality of a λ_2 signal at the destination node for different OXN system types. Although eye diagrams are deemed to be slightly inadequate for precise performance characterization of amplified optical networks [21], their use here for relative comparison of different OXN alternatives is sufficiently reliable. In figure 4, the eye diagrams for a

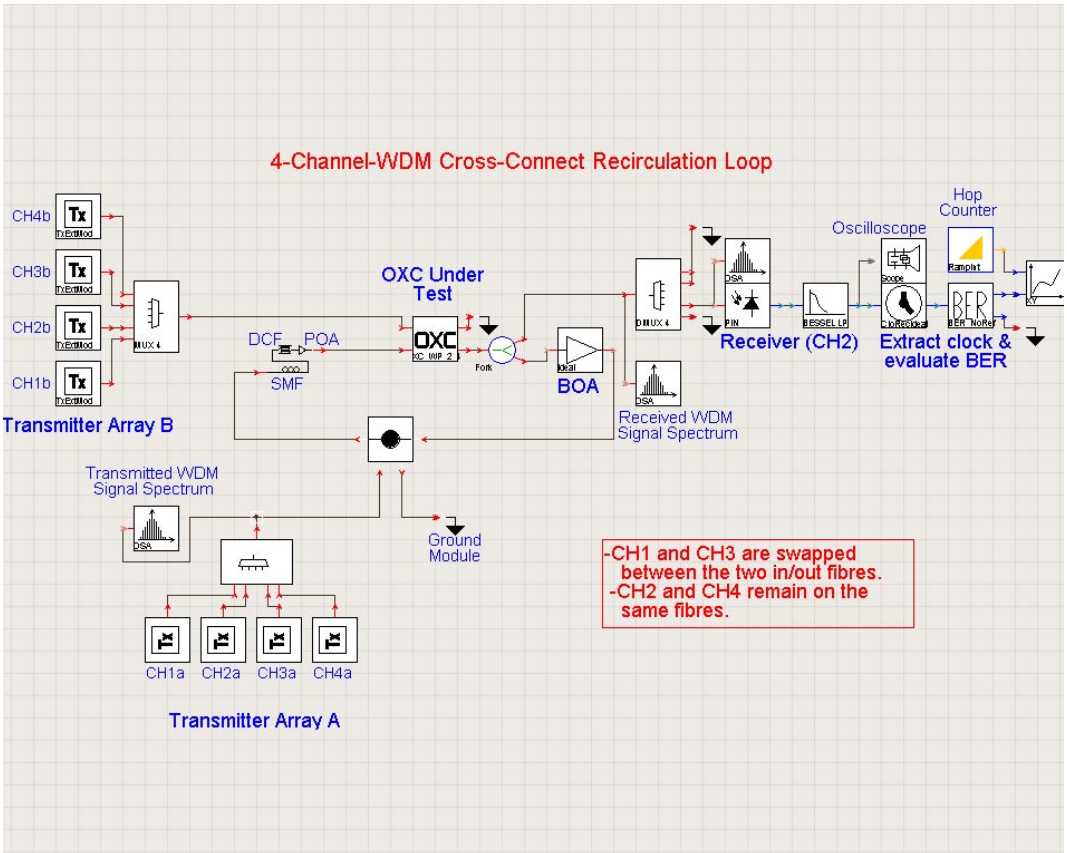

Figure 3. Simulation configuration of OXN circulating loop captured in a PTDS environment.

Table 1. Example nodes selected for performance comparison study.

Parameter	Unit	SMF	DCF
Length (L)	km	30.0	5.33
Attenuation coefficient (α)	dB km^{-1}	0.2	0.6
Dispersion (D)	ps nm^{-1} km^{-1}	16	−90
Dispersion slope (S)	s m^{-3}	80	210
Nonlinearity coefficient (γ)	m^2 W^{-1}	2.6×10^{-20}	4.0×10^{-20}
Effective core area (A_{eff})	μm^2	80	30

Table 2. Upper limits on the number of cascadable nodes considering stringent and lenient performance requirements.

OXN type	Performance requirement	
	Stringent	Lenient
OXN1	9	11
OXN2	4	6
OXN3	10	11
OXN4	9	11
OXN5	6	6
OXN6	5	6
OXN7	2	3
OXN2(Improved)	6	10
OXN7(Improved)	10	11

received λ_2 signal after seven nodes have been traversed to show the different example nodes described in section 2. It can be observed that in all cases the nodes have sufficient eye openings except for the systems using OXN2, OXN6 and OXN7 nodes. The almost complete eye closure in figure 4(g) is mainly attributed to the higher crosstalk penalties as a result of the use of MZI switches with a typically low isolation of 20 dB in OXN7 systems. This also seems to be the case with OXN6 systems (figure 4(f)), notwithstanding the fact that semiconductor optical amplifier (SOA) gates are used to improve the crosstalk isolation of MZI switches [14]. The SOA gates not only introduce signal dependent ASE and phase noise, but their gain also tends to saturate with surges in input power.

A more comprehensive performance indication of the node's transmission performance is obtained by using the PTDS BER module evaluating the Q factor and BER of the received λ_2 signal for path traversing up to 20 concatenated nodes. The results are depicted in figure 5 where the Q factor is expressed in dB ($Q_{\mathrm{dBfactor}} = 20\log(Q)$). The BER performance deteriorates with the node number, with the deterioration rate differing for each case due to different levels of accumulation of noise and crosstalk induced by each OXN type.

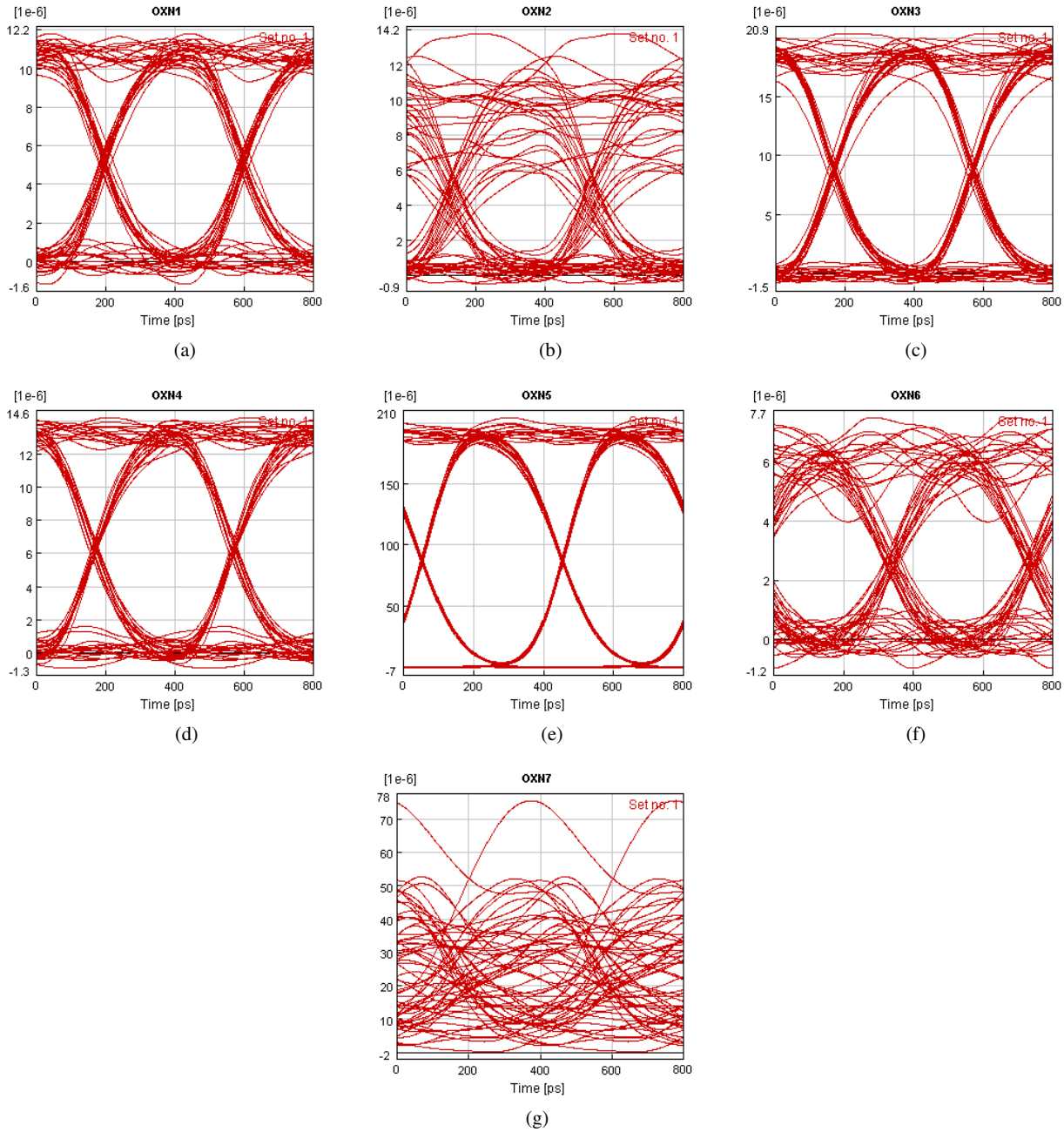

Figure 4. Eye diagrams for a received λ_2 signal after traversing seven nodes of type: (a) OXN1, (b) OXN2, (c) OXN3, (d) OXN4, (e) OXN5, (f) OXN6 and (g) OXN7.

Using the BER as the performance criterion for the decision process of an optical path request, the maximum number of cascadable nodes can be established for each node. Two performance-based optical path admission scenarios are considered with lenient and stringent Q factor requirements of 4.754 and 7.941 respectively (equivalent to BER of 10^{-6} and 10^{-15}). The lenient Q factor requirement could be used for systems that use error reduction techniques such as forward error correction [2, chapter 5].

From the results depicted in table 2, the best transmission performance is achieved by OXNs that are either dominated by passive optical devices (OXN5) or utilize novel switching technologies (OXN1, OXN3 and OXN4). The latter have been reported during or after 1998 and are generally characterized by fast switching times, low insertion loss and isolation in excess of 55 dB. Monolithically integrated OXNs realized on silica or InP substrates (OXN6, OXN7) offer favourable cost and size advantages, however, their transmission performance is significantly inhibited by high coupling losses to optical fibres and the presence of multiple low isolation MZI switches on the signal path. Recently, several improved designs for integrated nodes have been reported, these include the use of interferometric modulation devices for gate switches (MZI switch isolation increased to 30 dB [1]) or integrated OXN that avoid the use of MZI switches altogether [25]. Alternatively, space-switch structures based on a dilated Benes network made

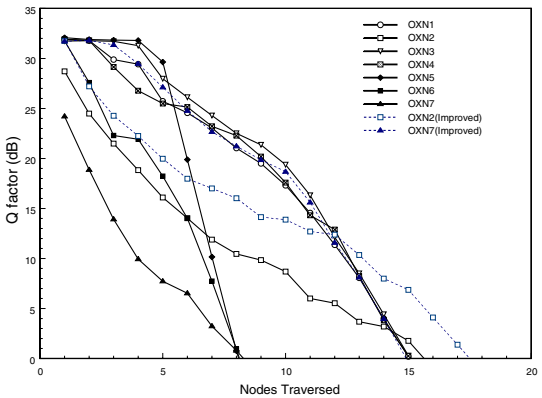

Figure 5. Simulated Q factor of the receieved λ_2 signal and different OXN types.

up of four 2×2 switches to form a single 2×2 switch have been proposed for both MZI switches (improving isolation by 20 dB [24]) and Ti:$LiNbO_3$ switches (isolation increased by up to 10 dB [26]). The transmission performance improvements that these modified switch structures provide to the OXN7 and OXN2 respectively are still well below the best performing OXNs for the case of OXN2 but improve the performance of OXN7 significantly (see figure 5 and table 2).

5. Conclusions

By using a commercially available photonic simulator, the comparison of the transmission performance of various optical network design alternatives was carried out. A simulation configuration based on an optical circulating loop offered a reduced computation time requirement, thus enabling the analysis of large cascades of OXNs. Based on the simulation results, we have concluded that the best 2×2 OXN architectures are those that are made up of polarization independent, low loss passive devices or novel switch fabrics. Alternative OXN designs that utilize both technologies for signal switching, multiplexing or demultiplexing purposes could offer even better cascadability performances. This is apparent in a node such as OXN5 that combines both integrated AWGs and passive fibre gratings and shows a marked improvement over traditional integrated nodes. Improvements in crosstalk isolation proposed for integrated OXNs still fall short of the transmission performance achieved by the aforementioned nodes.

Significant changes in performance can be expected for OXNs with a larger number of input/output fibres (e.g., 128 fibres) or a wavelength channel count that is at least an order of magnitude greater than that considered here [4]. The simulation of such nodes with larger dimensions can be carried out by capturing the node schematic in the PTDS environment by simply copying and pasting many 2×2 OXNs together. However, this is not possible for some node configurations, thus requiring the user to perform a painstakingly slow and tedious procedure of interconnecting hundreds of modules together to obtain a complete OXN structure. But it can still be argued that this is a price worth paying when one considers the possible cost (especially for discrete OXN architectures) of testing such large nodes in a laboratory. Judging from the significant influence exerted by the node-induced crosstalk penalties on the OXN cascadability performance, it seems necessary to adopt node configurations that contribute a low number intraband crosstalk components or to use some form of time-scheduled assignment of wavelength channels (such as that suggested in [27]) to reduce the likelihood of similar channels being cross-connected at the same time instant. The methodologies expounded here are equally applicable to other types of system-level simulators currently available.

References

[1] Yoshimura H, Sato K I and Takachio N 1999 *IEEE Commun. Mag.* **37** 74–81
[2] Ramaswami R and Kumar S N 1998 *Optical Networks: A Practical Perspective* (San Francisco, CA: Kaufmann) p 632
[3] Jackman N A, Patel S H, Mikkelsen B P and Korotky S K 1999 *Bell Labs Tech. J.* **4** 246–61
[4] Gillner L, Larsen C P and Gustavsson M 1999 *J. Lightwave Technol.* **17** 58–67
[5] Ciaramella E and Curti F 1999 *IEEE Photonics Technol. Lett.* **11** 751–3
[6] Iannone E and Sabella R 1996 *J. Lightwave Technol.* **14** 2184–96
[7] Roudas I, Antoniades N, Richards D H, Wagner R E, Jackel J L, Habiby S F, Stern T E and Elrefaie A E 2000 *IEEE J. Select. Topics Quantum Electron.* **6** 348–62
[8] Fouquet J E 1999 *Technical Digest of the Optical Fibre Communications Conf.* (Washington, DC: Optical Society of America) **1** Tu M1-1
[9] Johansson S, Lindblom M, Granestrand P, Lagerstrom B and Thylen L 1993 *J. Lightwave Technol.* **11** 688–94
[10] Laughlin R and Hazelton T 1998 *Proc. 11th IEEE Laser and Electro-Optics Society Annual Meeting* (New Jersey: IEEE) **2** pp 171–2
[11] Kenward M 2000 *FibreSystems Europe* **4** 37–9
[12] Marxer C and de Rooij N F 1999 *J. Lightwave Technol.* **17** 2–6
[13] Kim J, Jung J, Kim S and Lee B 2000 *Electron. Lett.* **36** 67–8
[14] Watanabe A, Okamoto S and Sato K I, 1996 *J. Lightwave Technol.* **14** 2162–72
[15] Kaneko A, Sugita A and Okamoto K 2000 *IEICE Trans. Electron.* **E 83-C** 860–8
[16] Herben C G P, Vreeburg C G M, Maat D H P, Leijtens X J M, Oei Y S, Groen F H, Pedersen J W, Demeester P and Smit M K 1998 *IEEE Photonics Technol. Lett.* **10** 678–80
[17] Lowery A, Vance R, Hewitt D, Harshavardhana P, Georgi S, Lenzmann O, Koltchanov I, Mooseburger R, Freund R, Richter A and Breuer D 2000 *Proc. of DesignCon 2000* (Los Angeles, CA: IEC) p 17
[18] Virtual Photonics Incorporated 2000 *VPI Ptolemy User's Manual* (Berlin: VPI) p 239
[19] Virtual Photonics Incorporated 2000 *Photonic Modules Reference Manual* (Berlin: VPI) p 778
[20] Agrawal G 1995 *Nonlinear Fibre Optics* (San Diego: Academic) p 592
[21] Ribeiro M R N, Waldman H, Klein J and Mendes L S 1997 *IEEE J. Select. Areas Commun.* **15** 707–16
[22] Liaw S K, Ho K P and Chi S 1997 *Electron. Lett.* **34** 1601–3
[23] Yoshimoto N, Shibata Y, Oku S, Kondo S and Noguchi Y 1998 *IEEE Photonics Technol. Lett.* **10** 531–3
[24] Maat D H P, Zhu Y C, Groen F H, van Brug H, Frankena H J and Leijtens X J M 2000 *IEEE Photonics Technol. Lett.* **12** 284–6
[25] Tzanakaki A, Guild K, Simeonidou D and O'Mahoney M J 1999 *Electron. Lett.* **20** 1755–6
[26] Pan Y, Qiao C and Yang Y 1999 *IEEE Commun. Mag.* **37** 50–6
[27] Subramaniam S, Harder E J and Choi H-A 2000 *IEEE J. Select. Areas Commun.* **18** 2105–10